Hindawi Publishing Corporation
Mathematical Problems in Engineering
Volume 2014, Article ID 101626, 12 pages
http://dx.doi.org/10.1155/2014/101626

Research Article

Design and Characteristic Analysis of a Novel Bearingless SRM considering Decoupling between Torque and Suspension Force

Yan Yang,[1] Zeyuan Liu,[1] Zhiquan Deng,[2] and Xin Cao[2]

[1] *College of Automation Engineering, Nanjing University of Posts and Telecommunications, Nanjing 210003, China*
[2] *College of Automation Engineering, Nanjing University of Aeronautics and Astronautics, Nanjing 210016, China*

Correspondence should be addressed to Yan Yang; yangyan0405@njupt.edu.cn

Received 17 July 2014; Revised 19 October 2014; Accepted 20 October 2014; Published 2 November 2014

Academic Editor: Ebrahim Momoniat

A Bearingless Switched Reluctance Motor (BSRM) has a complicated character of nonlinear coupling; therefore, it is a hard work to operate BSRM stably. In this paper, a new type of BSRMs with novel rotor structure is proposed by analyzing relationships between motor structure and theoretical formulae of levitation force and torque. The stator structure of this new motor is same as that of traditional BSRM and each stator pole can coil one winding or two windings, while the pole arc of rotor is wider. In order to analyze the characteristics of the proposed BSRM, finite-element (FE) models are used and a 12/4 one-set-winding BSRM and a 12/8 two-sets-windings BSRM are taken as examples. The analysis results indicate that the new scheme is effective for a stable levitation. It can realize decoupling control of torque and radial force, thus simplifying its control strategy and improving the use ratio of winding currents. A control system is designed for the 12/8 BSRM based on deducing its mathematical model. Compared with traditional BSRM, the proposed scheme is easier to be implemented.

1. Introduction

Because of the similarity between the structure of a magnetic bearing and that of a conventional switched reluctance motor (SRM), a Bearingless Switched Reluctance Motor (BSRM) integrates the magnetic suspension winding into a motor. It combines merits of a magnetic bearing and a conventional SRM such as ruggedness, low cost, fail-safe, no friction, no contact, high efficiency, fault-tolerance, and possible operation at high temperature; therefore, BSRM can operate at a high speed [1–3]. It has an advantage in a high-speed and super high-speed starter/generator for an advanced aircraft engine [4, 5]. Hence, it is expected to be suitable for commercial, industrial, and military applications.

According to the number of coil windings embedded in the stator, the BSRMs are divided into one set of windings and two sets of windings [6]. Both of the two motors produce unbalanced radial force by changing the air gap magnetic field density to realize the suspension of rotor. However, strong coupling exists between torque and levitation force in both traditional two-sets-windings BSRM and traditional one-set-winding BSRM. It is difficult to realize the complete decoupling of the two in the mathematical model and control strategy; thus, improvement of BSRM's levitating and rotating performance is limited. Scholars have done a lot of researches on the motor topology to solve the coupling problem and some research results have been obtained.

Scholars at Kyungsung University have proposed one method for two-phase BSRM with 8/10 or 12/14 hybrid pole type, in which each stator has one-set-winding. This proposal takes advantage of the hybrid structure of narrow and wider teeth to separate the radial force stator pole from the torque stator pole [7–10]. Levitation force and torque are produced separately by suspension winding and torque winding, thus realizing the natural decoupling of torque and levitation. However, the wider stator teeth occupy a large space, and the operation of motor is two-phase excitation, which limits the output of power density. Moreover, the number of rotor poles is larger than the number of stator poles, so it is difficult to improve the high speed performance.

NASA Glen Research Center proposed a one-set-winding BSRM with hybrid rotor, which consists of two parts: circular

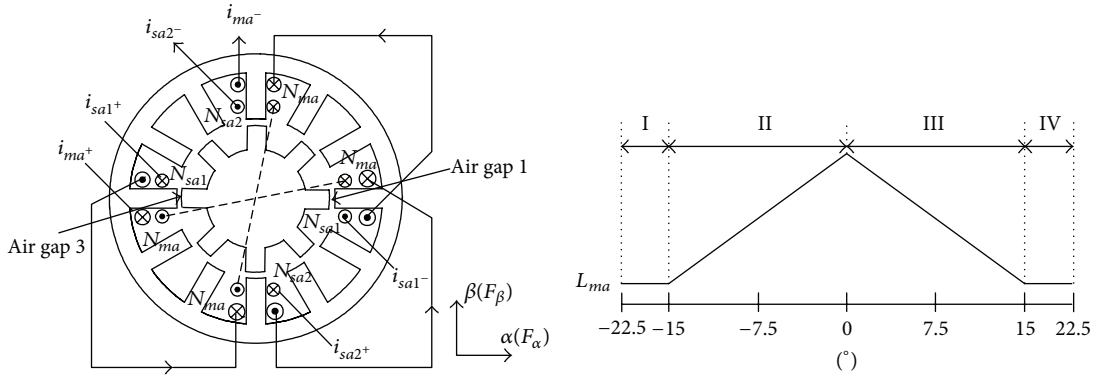

(a) Configuration (b) Inductance curve

Figure 1: Configuration and inductance curve of traditional 12/8 BSRM.

and scalloped lamination segments [11, 12]. When controlling in practice, coils of one set of four stator poles form a set of windings, providing levitation force for the circular laminated section of rotor and playing the role of the magnetic bearing to levitate the rotor. The other set of four stator poles imparts torque to the scalloped portion of the rotor. The motor of this structure is easy to control, but its biggest shortcoming is that same as the magnetic bearing motor system and the axial length is longer, which limits the critical speed of rotor.

The high-speed motor research center of Nanjing University of Aeronautics and Astronautics improves the suspension winding arrangements of traditional 12/8 BSRM with two-sets-windings, proposing a three-phase, two-sets-windings, 12/8 series-excited BSRM [13], which connect the traditional three-phase suspension winding in the same direction in series to become a one-set-winding. Thus it makes the suspension winding inductance unchanged at one rotor cycle. The suspension current does not produce torque, which realizes the decoupling control of torque and levitation force. Nevertheless, since the demand for copper wire of suspension winding is high, it is wasteful and causes the utilization rate of winding to be lower.

In this paper, a new type of BSRM with novel rotor structure is proposed based on 12/8 two-sets-winding BSRMs and 12/4 one-set-winding BSRMs. The scheme uses wider pole arcs in the rotor and makes the winding inductance curve a flat area in the inductance maximum position, thus realizing decoupling control of the levitation force and torque. First, the structure characteristics of the proposed BSRM are summed up by analyzing relationships between torque, suspension force, and inductance. Then, operating principle of the new structure BSRM is illustrated. Accordingly, the torque and suspension force performances of the proposed BSRM are analyzed in detail with finite-element (FE) calculation. Mathematical model for suspension force is deduced and a control system is designed for the 12/8 BSRM with two-sets-windings. Compared with traditional BSRM, the proposed scheme has a simpler suspension force model and is easier to be controlled; besides, it can realize decoupling between torque and radial force.

2. Characteristics and Analysis of Traditional BSRM

Figure 1(a) shows the configuration of the traditional 12/8 BSRM with only phase-A winding [14]. The pole arcs of the stator and rotor are both equal to 15 mechanical degrees (°M). The aligned position is defined as $\theta = 0$°M. There are two kinds of stator windings: the motor main winding and radial force windings. The main winding N_m consists of four coils connected in series. Each radial force winding N_s consists of two coils. When the two differential windings conduct the currents as shown in Figure 1(a), the flux density in air gap 1 increases, whereas it decreases in air gap 3. Thus, an unbalanced magnetic force is produced toward the positive direction in the α-axis. Radial force toward the β-axis can also be produced in the same way. Therefore, radial force in any desired direction can be produced by composing the two radial forces in perpendicular directions. Because the number of rotor poles is 8, the inductance cycle of winding is 45°M. Figure 1(b) shows the form of the main winding self-inductance curve.

The stored magnetic energy W_a in phase-A can be expressed as [14, 15]

$$W_a = \frac{1}{2}\begin{bmatrix} i_{ma} & i_{sa1} & i_{sa2} \end{bmatrix} \times \begin{bmatrix} L_a \end{bmatrix} \times \begin{bmatrix} i_{ma} \\ i_{sa1} \\ i_{sa2} \end{bmatrix}. \tag{1}$$

The inductance matrix $\begin{bmatrix} L_a \end{bmatrix}$ of phase-A is a 3 × 3 matrix constructed by self and mutual inductances and it can be written as

$$\begin{bmatrix} L_a \end{bmatrix} = \begin{bmatrix} L_{ma} & M_{(ma,sa1)} & M_{(ma,sa2)} \\ M_{(ma,sa1)} & L_{sa1} & M_{(sa1,sa2)} \\ M_{(ma,sa2)} & M_{(sa1,sa2)} & L_{sa2} \end{bmatrix}, \tag{2}$$

where L_{ma}, L_{sa1}, and L_{sa2} are the self-inductances of N_{ma}, N_{sa1}, and N_{sa2}, respectively; $M_{(ma,sa1)}$ is the mutual inductance between N_{ma} and N_{sa1}; $M_{(ma,sa2)}$ is the mutual inductance between N_{ma} and N_{sa2}; and $M_{(sa1,sa2)}$ is mutual inductance between N_{sa1} and N_{sa2}.

According to the principle of electromechanical energy conversion, the torque T_a due to phase-A can be written as

$$T_a = \frac{\partial W_a}{\partial \theta} = \frac{\partial \left((1/2) \left[L_{ma} i_{ma}^2 + L_{sa1} i_{sa1}^2 + L_{sa2} i_{sa2}^2 \right] \right)}{\partial \theta}. \quad (3)$$

When the shaft has no load or light load in its radial direction, the suspension current value will be very small because a small levitation force is needed to maintain rotor stable suspension in that case. Therefore, the contribution of suspension winding currents on the torque can be ignored. The torque T_a can be expressed as a linearized model:

$$T_a = \frac{1}{2} \frac{\partial L}{\partial \theta} i_{ma}^2. \quad (4)$$

In the same way, suspension forces in two directions produced by the current in phase-A can be obtained by the virtual displacement method and can be written as

$$\begin{aligned} F_\alpha &= \frac{\partial W_a}{\partial \alpha} = \frac{\partial \left(M_{(ma,sa1)} i_{ma} i_{sa1} + M_{(ma,sa2)} i_{ma} i_{sa2} \right)}{\partial \alpha} \\ &= K_f(\theta)\, i_{ma} i_{sa1}, \\ F_\beta &= \frac{\partial W_a}{\partial \beta} = \frac{\partial \left(M_{(ma,sa1)} i_{ma} i_{sa1} + M_{(ma,sa2)} i_{ma} i_{sa2} \right)}{\partial \beta} \\ &= K_f(\theta)\, i_{ma} i_{sa2}, \end{aligned} \quad (5)$$

where $K_f(\theta)$ is a proportional coefficient of radial force; it is a function of the rotor position angle θ and the dimensions of BSRM [14–17].

It is known from (4) that the torque is proportional to the partial derivative of the main winding inductance to rotor position angle. As shown in Figure 1(b), the inductance in Sections 1 and 4 is constant. Therefore, the winding current does not generate torque in these two regions. The current conducted in Section 2 produces positive torque, while the current conducted in Section 3 produces negative torque. In practice, it can realize torque control by adjusting the conduction width of Sections 2 and 3 flexibly according to the load torque.

We can also see from (5) that the magnitude of suspending force is proportional to the coefficient $K_f(\theta)$ and winding currents. For improving the use ratio of currents, a large$K_f(\theta)$ is needed to generate certain suspension force. If rotor and stator poles are aligned, $K_f(\theta)$ obtains a large value for the magnetic reluctance of air gap which is minimum at this angle position. As the rotor rotates away from the aligned position, $K_f(\theta)$ value becomes less because of the increase in magnetic reluctance causing a decrease in air gap flux. Therefore, the turn-ON angle should be shifted toward aligned position to improve the suspension performance. That is to say, in Figure 1(b), suspension force should also be generated in intervals II and III around aligned position. So, the suspension force has nonlinear character and coupled with torque. It is complicated to calculate the suspension force value for position-dependent $K_f(\theta)$ and currents. This will make algorithm more complex and demand higher requirements upon digital controller. Meanwhile, large negative torque will be produced when the currents conduct in region III, which will lead to low-usage of winding current and limit speed performance.

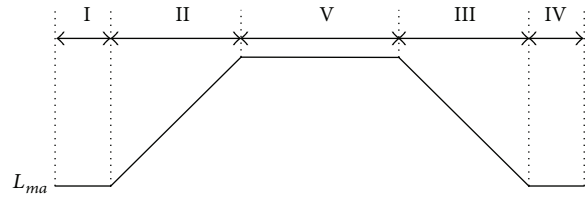

Figure 2: The aim form of inductance curve.

3. Structure Characteristics and Operating Principles of the Novel BSRM

According to the above analysis of traditional BSRM, the proportional coefficient $K_f(\theta)$ and inductance L_{ma} obtain their maximum values in aligned position at the same time. Thus, if changing the structure of the motor can generate a flat area in the winding inductance curve located in the inductance maximum position, then it will only generate a large and linear suspension force but fails to produce torque, if the motor in this flat area is excited. Then the winding inductance curve has the form as shown in Figure 2. The suspension force of motor can be controlled in region V and the torque can be controlled in the inductance rising region II. BSRMs with this new inductance feature, whose suspension force will be linear and this scheme is undesired to compromise between torque and radial force; furthermore, no negative torques are generated. So, it may improve the efficiency of winding currents and will be easier to be controlled.

3.1. Structure Characteristics of Novel BSRMs. On the premise of the fact that the stator structure of the new BSRM is same as the stator structure of traditional BSRM, we increase the width of rotor pole. The rotor pole arc will be greater than the stator pole arc. We name it wider-rotor-teeth BSRM. The reason to do so is that when the stator and rotor pole of the motor are in aligned position, the proportional coefficient $K_f(\theta)$ and the inductance of winding reach their maximums; hence, increasing overlap area of the rotor and stator pole during rotor rotation by increasing the width of rotor pole can produce the flat area of the inductance. Based on this principle, when it comes to a m-phase motor whose rotor teeth number is N_r, one rotor cycle angle will be $(360/N_r/m)^\circ$M. So the region where suspension forces are generated is $(360/N_r/m)^\circ$M; m phases conduct in turn to provide steady suspension forces. Therefore, it requires that the inductance curve in the maximum inductance has a flat area of $(360/N_r/m)^\circ$M at least to provide stable suspension force for rotor and to realize decoupling control of the torque

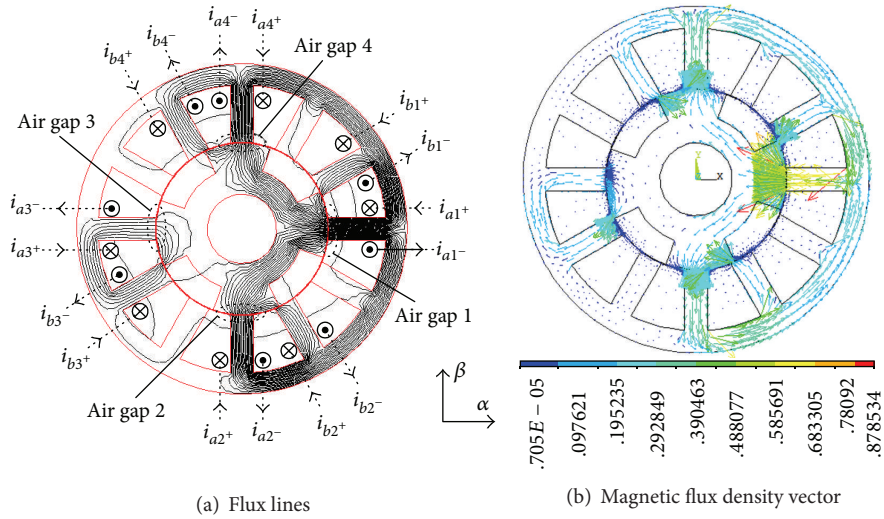

(a) Flux lines (b) Magnetic flux density vector

Figure 3: Configuration and operating principle of 12/4 BSRM with one set of windings.

and the suspension force. Thus, the relationship between rotor pole arc angle and stator pole arc angle must satisfy

$$\beta_r \geq \beta_s + \frac{360^\circ}{m \cdot N_r}, \tag{6}$$

where β_r and β_s are the rotor pole arc angle and the stator pole arc angle, respectively. N_r is the number of rotor poles.

The structure of wider-rotor-teeth BSRM not only can be two-sets-winding BSRM but also can be one-set-winding BSRM.

3.2. Operating Principles of Novel BSRM. Taking a 12/4 structure with wider-rotor-teeth and one set of windings BSRM and a 12/8 structure with wider-rotor-teeth and two sets of windings BSRM as examples, this section introduces the rotation operation principle of the novel BSRM.

3.2.1. 12/4 BSRM with One Set of Windings and Wider-Rotor-Teeth. Figure 3 shows the configuration of the 12/4 wider-rotor-teeth BSRM with only A-phase and B-phase windings. The arc angle of stator pole is still 15°M as traditional BSRMs, and each stator tooth is embedded in one set of concentrated windings. Four windings of each phase are controlled independently. According to (6), the arc angle of rotor pole should be not less than 45°M, and here the minimum value 45°M is taken. In Figure 3, phase-A is at the maximum inductance position. When the two windings of phase-A in the α-direction adopt asymmetric excitation, as shown in Figure 3, the flux density in air gap 1 increases, whereas it decreases in air gap 3. Therefore, an unbalanced magnetic force acting on rotor F_α is produced toward the positive direction in the α-axis. The radial force F_β in the β-axis can also be produced in the same way. Thus, radial force in any desired direction can be produced by composing the two radial forces in perpendicular directions. This principle can be similarly applied to the phase-B and phase-C windings.

Obviously, because phase-A is in the flat area of maximum inductance as the rotor position shown in Figure 3, it only generates suspension force but generates no torque. Therefore, it is necessary to turn-ON windings of two phases at the same time to realize stable operation: one in the flat area of inductance to generate suspension force, another in the inductance rising to generate torque. Taking counter-clockwise as the positive orientation, phase-B in Figure 3 is just in inductance rising region. Torque for motor's rotation can be generated by exciting the four windings of phase-B symmetrically.

3.2.2. 12/8 BSRM with Two Sets of Windings and Wider-Rotor-Teeth. The number of coil windings embedded in the stator can also be two sets. A three-phase 12/8 BSRM with proposed novel rotor was taken as example to illustrate the suspension and operation principle of the BSRM with two sets of windings. Figure 4 is the configuration of the novel BSRM, which has two sets of windings and wider-rotor-teeth. The arc angle of stator pole is still 15°M, and each stator pole is embedded in two sets of concentrated windings. The windings arrangement is the same as that of the traditional 12/8 two-sets-windings BSRM. Figure 4 only gives the two sets of windings of phase-A and the main winding of phase-C. According to (6), the pole arc of rotor is designed as 30°M.

Similar to 12/4 BSRM above, it is necessary to turn-ON two phase windings at the same time. One phase winding is used to generate radial force, while the other phase winding is used to generate torque. In Figure 4, the main winding of phase A adopts symmetric excitation and conducts current i_{ma}. The current i_{sa1} of radial force winding enhances the flux density in air gap 1 and reduces it in air gap 3. Therefore, controllable radial force to levitate rotor is generated in α-direction. The radial force in the β-axis can also be produced

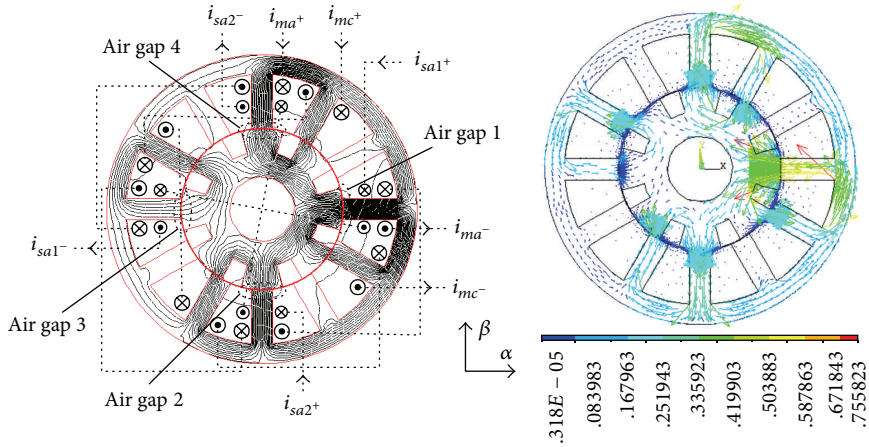

(a) Flux lines (b) Magnetic flux density vector

FIGURE 4: Configuration and operating principle of 12/8 novel BSRM with two sets of windings.

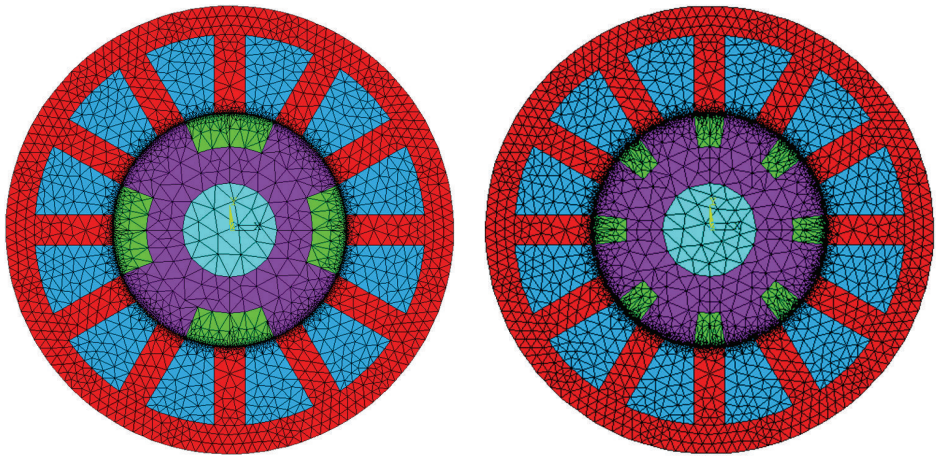

(a) 12/4 BSRM (b) 12/8 BSRM

FIGURE 5: 2D FE mesh models of 12/4 BSRM and 12/8 BSRM.

in the same way. Radial force in any desired direction can be produced by composing the two radial forces in α and β directions. The torque for motor's rotation is generated by symmetrically exciting main winding of phase-C, because phase-C is just in inductance rising region at this moment.

4. Electromagnetic Analysis of Two Wider-Rotor-Teeth BSRMs

In order to verify the validity of the suspension operation principles and provide the basis theory for motor control strategy, the above two kinds of wider-rotor-teeth structure BSRM are analyzed through FE method. In order to facilitate the comparison between the two prototypes, the same rated condition is adopted here. The rated power is 2 kW, the rated speed is 20000 r/min, and the maximum radial force is 100 N. The dimensions of the simulation motors are shown in Table 1.

The software of Ansys is used to calculate electromagnetic field. The 2-dimensional (2D) FE models of 12/4 BSRM and 12/8 BSRM are established and their 2D FE mesh models are shown in Figure 5. We use enhanced incremental energy method to calculate inductances of winding, since it only needs to calculate incremental energy without the need for system energy [18].

For a single loop magnetic system, if the operating current of the loop is i_0, the static inductances L can be calculated by

$$L = \frac{\Psi}{i_0} = \frac{\Delta W_C}{i_0 \Delta i}, \tag{7}$$

where ΔW_C is the magnetic field coenergy increment, i_0 is current pass through the magnetic loop, Ψ is the flux linkage, and Δi is the increment of i_0.

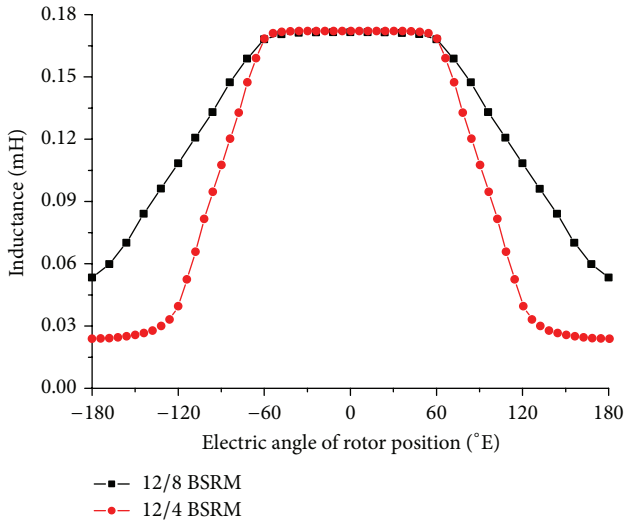

Figure 6: Inductances of 12/4 and 12/8 wider-rotor-teeth BSRMs.

Table 1: Parameters of 12/4 and 12/8 wider-rotor-teeth BSRMs.

Stator diameter/mm	95
Rotor diameter/mm	49.8
Stator yoke/mm	6.1
Rotor yoke/mm	7.65
Stator pole height/mm	16.5
Rotor pole height/mm	7
Stator pole arc/°M	15
Diameter of axle/mm	20
Gap length/mm	0.25
Length of stator stack/mm	55
Rotor pole arc of 12/4 BSRM/°M	45
Number of windings of 12/4 BSRM	13
Rotor pole arc of 12/8 BSRM/°M	30
Number of main windings of 12/8 BSRM	9
Number of suspension windings of 12/8 BSRM	13

The increment of magnetic field coenergy ΔW_C can be calculated as

$$\Delta W_C = \int B(\Delta H)\, dV, \tag{8}$$

where B is flux density and ΔH is the magnetic field increment.

Then, combining (7) and (8), inductances can be written as

$$L = \frac{\int B(\Delta H)\, dV}{i_0 \Delta i}. \tag{9}$$

4.1. FE Analysis Results with Only Phase-A Excited. To the 12/8 BSRM shown in Table 1, the given currents conducted in main winding and suspension winding are $i_{ma} = 5$ A, $i_{sa1} = 3.6$ A, and $i_{sa2} = 0$, respectively. To the 12/4 BSRM, the given currents are $i_{a1} = 8.6$ A and $i_{a2} = 1.4$ A. The main winding inductances of phase-A are calculated. Figure 6 shows relationships between inductance and the rotor position angle of two kinds of BSRM. For the purposes of comparison, here, all the actual position mechanical angles of rotor were multiplied by the respective number of rotor teeth, so that each cycle of rotor angle corresponding to the motor becomes 360 electrical degrees (°E). It can be seen from Figure 6 that the winding inductances of the two kinds of BSRM are all about constant maximum values in the interval [−60°E, 60°E], this is consistent with the results of theoretical analysis, and the inductance curve has the same shape as shown in Figure 2.

Figure 7 shows relationships suspension force, or instantaneous torque and the rotor position angle of two kinds of BSRM, respectively. Figure 7(a) shows that the maximum levitation force can also be obtained in [−60°E, 60°E] interval, while the torque is basically 0 in this interval as shown in Figure 7(b). That is to say, there is large suspension force produced while it fails to produce torque in this region. Figure 7(b) also shows that torques are generated in the inductance rising and drop region. The levitation force and torque produced in different regions; thus, it can realize the decoupling control of torque and levitation force. This result is in agreement with theoretical result.

The results also show that the output torque width of 12/4 BSRM is only 1/2 of the output torque width of 12/8 BSRM, so the torque angle characteristic of 12/8 BSRM is better. The 12/4 BSRM is more suitable for light load applications.

4.2. FE Analysis Results with Two Phases Excited Simultaneously. Keep the phase-A currents in [−60°E, 60°E] region the same as that in former simulation. phase-A produces larger suspension force while it fails to produce torque according to the analysis of previous section. To the 12/4 BSRM, the currents of phase-B were conducted to produce torque since the inductance of phase-B is just rising in this region. Given currents conducted in phase-B are $i_{b1} = i_{b2} = 5$ A. In the same way, to the 12/8 BSRM, the conduction of phase-C to produce torque and the given current is $i_{mc} = 5$ A. Figure 8 shows the FE analysis results of suspension force and torque. It can be seen that no matter two phases excited simultaneously or only phase-A excited, the suspension force is approximately the same. The values of two phases excited are slightly larger than that of only one phase excited, but the difference is less than 4%. Thus the effects of phase-B or phase-C conduction to levitation forces can be ignored in the two BSRMs. It can also be seen from Figure 8 that torque values are approximately zero with only phase-A conducted, while they greatly increased when two phases excited simultaneously. Compared with Figure 7, the generated torque values of the two motors are all very close to those of only one phase conducted in their inductance rising region. The difference is also less than 4%. Thus the torque generated by the phase, which mainly produces the suspension force, can be ignored.

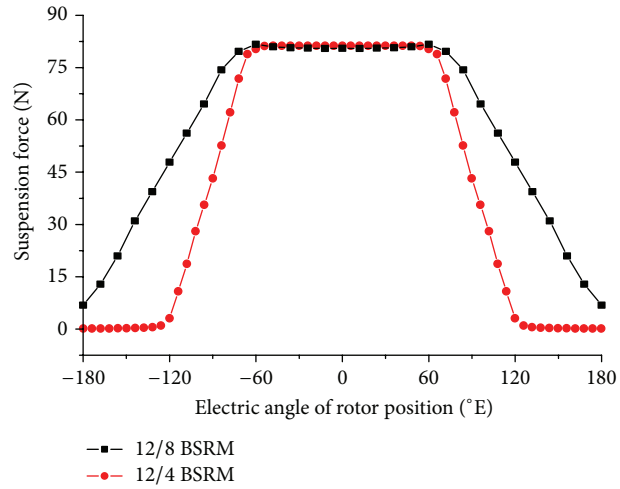

(a) Suspending forces at α-direction

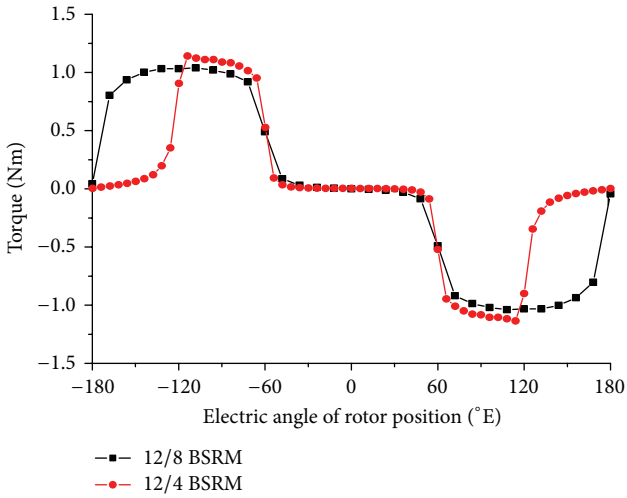

(b) Torques

FIGURE 7: Suspension forces and torques of 12/4 and 12/8 wider-rotor-teeth BSRMs.

That is to say, the coupling effect between phase and phase can be ignored.

5. System Analysis of Two Wider-Rotor-Teeth BSRMs

5.1. Mathematical Model of 12/8 BSRM. The radial suspension force and torque acting on rotor should be acquired in order to control the BSRM. This paper derives the mathematical model through virtual displacement method as traditional BSRM [14, 19]. The current of suspension winding conducts in the interval [−7.5°M, 7.5°M] where the stator teeth and the rotor teeth are always overlapped. It can be seen from Figure 4 that the magnetic field lines are almost perpendicular from the rotor teeth to the stator teeth in this area, while the fringing flux is small and can be ignored. Therefore, the magnetic circuit diagram of the magnetic circuit can be represented as straight lines as shown in Figure 9.

Accordingly, the magnetic permeance can be expressed as

$$P = \frac{\mu_0 hr\pi}{12l_0}. \tag{10}$$

Here, μ_0 is the permeability in the air, h is the axial length of stator, r is the radius of rotor, and l_0 is the average air gap length.

The levitation force in two directions and the torque can also be obtained by the virtual displacement method. Equation (10) shows that the permeance is only decided by dimensions of BSRM; therefore, the proportional coefficient $K_f(\theta)$ of radial force in (5) becomes a constant and the suspension force mathematical model for novel motor becomes

$$\begin{aligned} F_\alpha &= K_f i_{ma} i_{sa1}, \\ F_\beta &= K_f i_{ma} i_{sa2}, \end{aligned} \tag{11}$$

where the proportional coefficient K_f is a constant and can be expressed as

$$K_f = \frac{\mu_0 hr\pi}{6l_0^2} N_m N_s. \tag{12}$$

Also according to the principle of virtual displacement, the instantaneous torque of phase A can be expressed as

$$T_a = J_t(\theta)\left(2N_m^2 i_{ma}^2 + N_s^2 i_{sa1}^2 + N_s^2 i_{sa2}^2\right). \tag{13}$$

In inductance rising region, the positive torque coefficient can be expressed as

$$J_{tp}(\theta) = \mu_0 hr\left[\frac{1}{l_0} - \frac{4l_0 - 1.28\pi r\theta}{(2l_0 - \pi r\theta)^2}\right]. \tag{14}$$

It can be seen from (11) and (12) that suspension forces in suspension region are simply determined by winding currents after motor structure parameters have been determined, which are independent of rotor position angle. Thus, they can be easier controlled than that in traditional case. In practice, if there is a positive or negative eccentric displacement x in α-direction or β-direction, the average air gap l_0 will be revised to $l_0 \mp x$ in (11) and (13).

5.2. Control Scheme. Figure 10 illustrates the principle of the proposed control scheme. The rotor pole arc angle is 15°M larger than the stator pole arc according to the above analysis of 12/8 BSRM, which forms a 15°M maximum flat area of windings inductance within [−7.5°M, 7.5°M]. The proposed scheme fixes the width of radial force winding currents just at [−7.5°M, 7.5°M] area, shown as region I in Figure 10. The combination of the main winding and suspension winding currents in this region I produces larger and consecutive radial force to levitate rotor. However, the instantaneous torque within region I is approximately equal to 0. The suspension winding does not conduct in any nonoverlapping

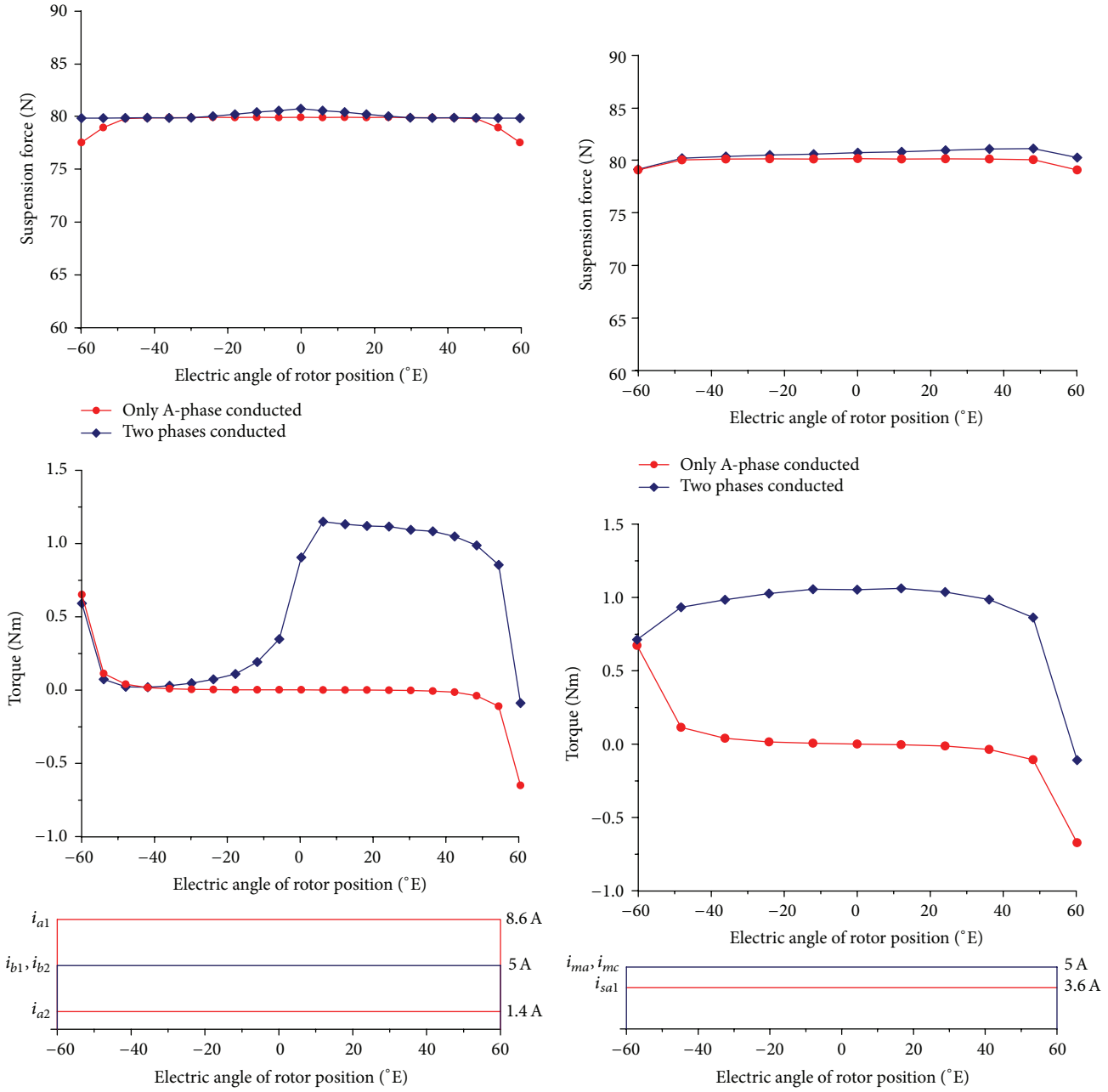

(a) 12/4 BSRM (b) 12/8 BSRM

Figure 8: Suspension forces and torques with two phases excited simultaneously.

area, whereas the main windings are also excited in the interval [−22.5°M, −7.5°M] to generate torque. Thus, region I and region II are used to control suspension force and torque, respectively, which can realize the decoupling control of torque and suspension force. In practice, the turn-ON angle of main windings can be adjusted according to the requirements of actual average torque. To obtain a larger average torque, we can advance the turn-ON angle of main winding currents as much as possible. The waveforms of currents can also be changed by the corresponding control objectives, such as higher efficiency and lower vibration. In Figure 10, the turn-ON angle and waveform of main windings are selected as −15°M and square-wave, respectively.

5.3. Block Diagram of Control System. According to the above analysis, the control system can be made according to Figure 11 during practice. After the rotor's location is detected through the encoder, the real-time rotation speed of the motor can be got through location computation. The difference between it and the given speed is formed

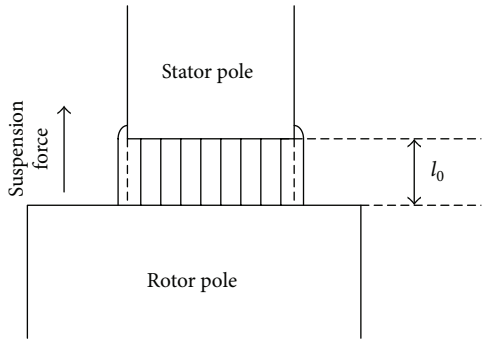

Figure 9: Magnetic circuit diagram.

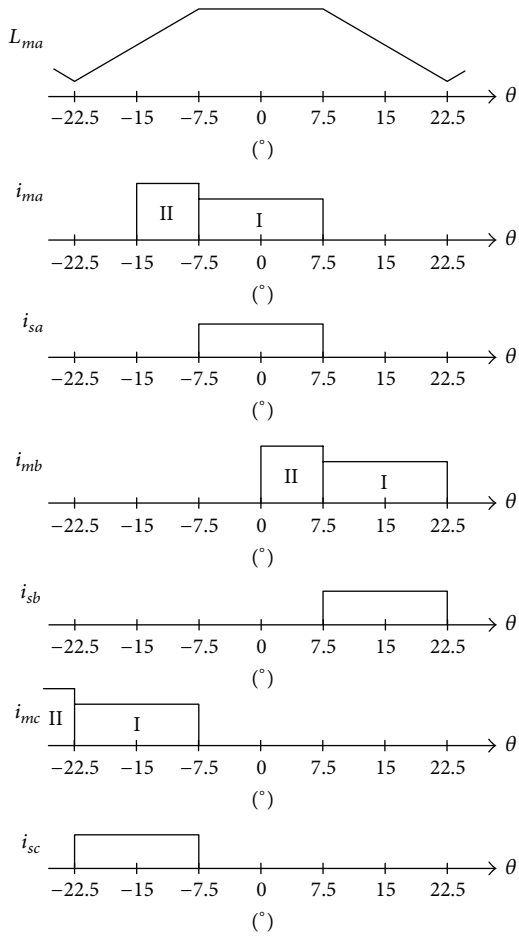

Figure 10: Control scheme of new 12/8 BSRM.

as the active phase current $i_{m1}{}^*$ through the PI controller. The rotor radial displacements at the two perpendicular directions are measured and converted into electrical signals through the radial displacement sensor and are output as the desired radial forces $F_\alpha{}^*$ and $F_\beta{}^*$ after the PID controller. Based on the desired value, according to the corresponding control targets and (11), the currents $i_{m2}{}^*$, $i_{s1}{}^*$, and $i_{s2}{}^*$ in the suspension interval can be computed. Finally, the stable suspension during the operation of the motor can be achieved by tracing the set value of currents through the power controllers on the two windings.

5.4. Simulation and Analysis. The 12/8 BSRM dimensions of the simulation motor are the same as shown in Table 1. The given radial force in α-axis is 50 N, whereas it is 30 N in the β-axis. Figures 12(a) and 12(b) show simulation waveforms of the currents, torque, and levitation forces under giving the main winding turn-ON angle θ_{on} equal to –15°M and –22.5°M, respectively. Here, the currents are controlled as square-wave. It can be seen that the change of the turn-ON angle makes the output average torque change. When the angle θ_{on} is advanced, the output average torque is increased. So the output of average torque can be controlled by adjusting the turn-ON angle of the main winding. However, due to the winding inductance, the main winding current in the torque production section cannot be rapidly converted into the current required by the suspension section, and a delay exists, as shown in the area circled by broken lines in Figure 12. As a result, the suspension forces cannot track their given values well during currents conversion area. To solve this problem, it is necessary to add a compulsive excitation unit to the main winding converter. That is, by applying an inverse voltage when the current changes, rapidly convert the current of main windings to the value required by the suspension section. Figure 13 shows the simulation waveforms of the currents, torque, and levitation forces. As can be seen from Figures 13(a) and 13(b), after the compulsive excitation unit is added, the suspension force was well tracked.

6. Conclusions

This paper studied a new-structure BSRM, which adopts a wide rotor pole structure. The nonlinear FEM and system simulation analysis based on MATLAB are used to analyze the performance of the novel motor. Analysis results of two prototypes indicate that

(1) the novel BSRM has linear mathematical model of suspension force, since it can produce a flat area at the position of maximum inductance on the winding inductance curve;

(2) the novel BSRM can realize decoupling control of torque and suspension force. Therefore, the algorithm is easier to be implemented and demands lower requirements upon digital controller;

(3) since no negative torques are generated in control, the availability of winding current is higher than traditional case;

(4) to avoid the problem of poor suspension force performance caused by current delay during converting the main winding currents from torque production region to suspension force production region, it is necessary to add a compulsive excitation unit into the converter of the main winding.

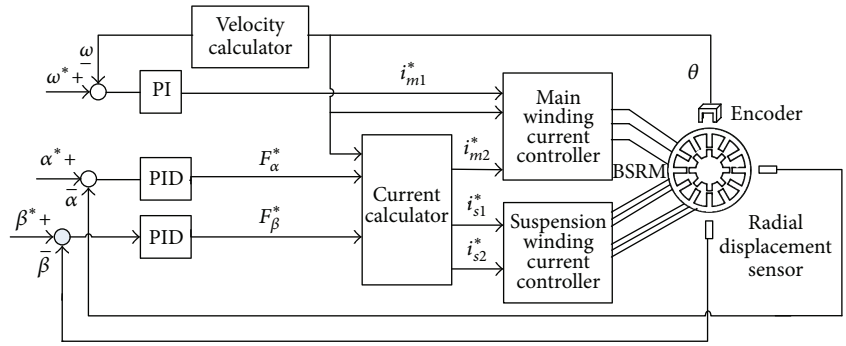

Figure 11: Block diagram of control system.

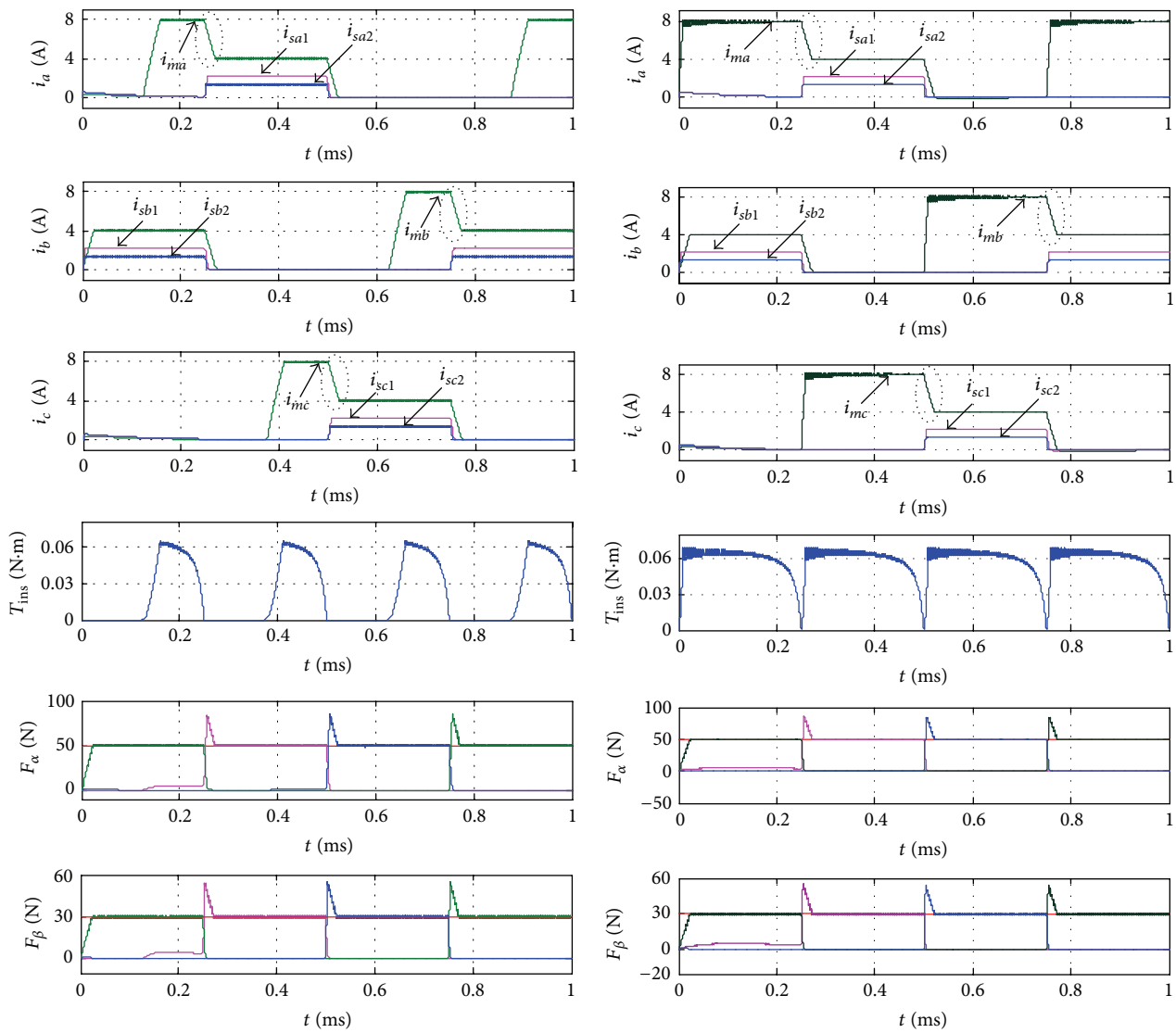

(a) $\theta_{on} = -15^{\circ}$ M (b) $\theta_{on} = -22.5^{\circ}$ M

Figure 12: Simulation waveforms of the currents, torque, and levitation forces without compulsive excitation unit.

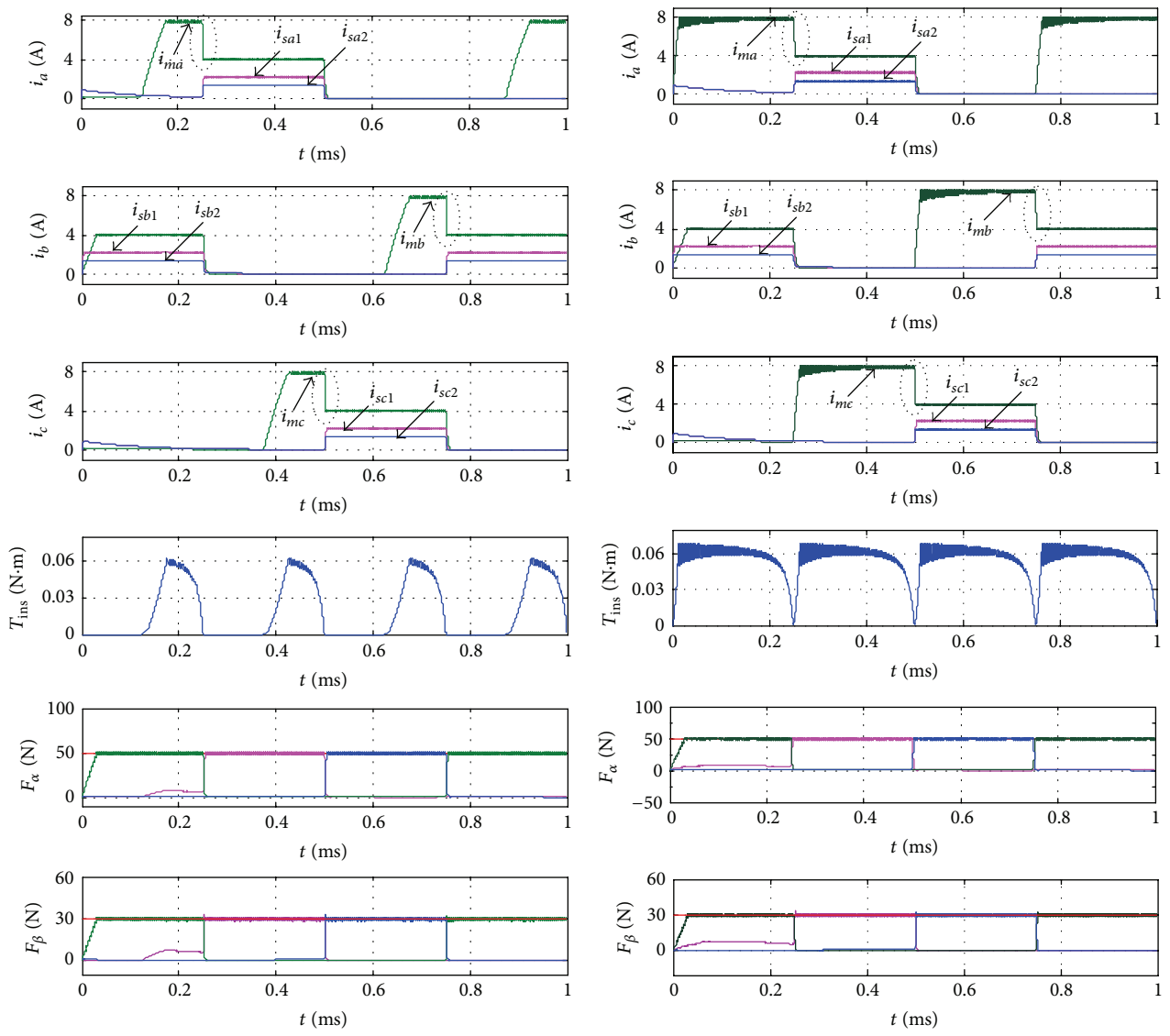

(a) $\theta_{on} = -15^\circ$ M (b) $\theta_{on} = -22.5^\circ$ M

FIGURE 13: Simulation waveforms of the currents, torque, and levitation forces after compulsive excitation unit is added.

Conflict of Interests

The authors declare that there is no conflict of interests regarding the publication of this paper.

Acknowledgments

This study was cosupported by the National Natural Science Foundation of China (no. 51207073) and the scientific research fund of Nanjing University of Posts and Telecommunications (no. NY211021).

References

[1] T. Higuchi, H. Kawakatsu, and T. Iwasawa, "A study on magnetic suspension of switched reluctance motor," in *Proceedings of the Conference Record of the IEEE Industry Applications Society Annual Meeting*, vol. 6, pp. 122–123, Tokyo, Japan, 1989.

[2] J. Bichsel, "The bearingless electrical machine," in *Proceedings of the International Symposium on Magnetic Suspension Technology*, pp. 561–573, Hampton, Va, USA, NASA Langley Research Center, 1991.

[3] T. Fukao, "The evolution of motor drive technologies. Development of bearingless motor," in *Proceedings of the 3rd International Power Electronics and Motion Control Conference*, pp. 33–38, Beijing, China, January 2000.

[4] Y. Gang, Z. Deng, X. Cao, and X. Wang, "Optimal winding arrangements of a bearingless switched reluctance motor," *IEEE Transactions on Power Electronics*, vol. 23, no. 6, pp. 3056–3066, 2008.

[5] Y. Yang, Z. Deng, Q. Zhang, Z. Liu, and X. Cao, "Effects of control strategies on stator vibration of bearingless switched

reluctance motors," *Acta Aeronautica et Astronautica Sinica*, vol. 31, no. 10, pp. 2010–2017, 2010 (Chinese).

[6] Y. Yang, Z. Deng, G. Yang, X. Cao, and Q. Zhang, "A control strategy for bearingless switched-reluctance motors," *IEEE Transactions on Power Electronics*, vol. 25, no. 11, pp. 2807–2819, 2010.

[7] W. Huijun, L. Dong-Hee, and A. Jin-Woo, "Novel bearingless switched reluctance motor with hybrid stator poles: concept, analysis, design and experimental verification," in *Proceedings of the 11th International Conference on Electrical Machines and Systems*, pp. 3358–3363, Wuhan, China, October 2008.

[8] D.-H. Lee, H. Wang, and J.-W. Ahn, "Modeling and control of novel bearingless switched reluctance motor," in *Proceedings of the IEEE Energy Conversion Congress and Exposition (ECCE '09)*, pp. 276–281, San Jose, Calif, USA, September 2009.

[9] X. Zhenyao, L. Dong-Hee, Z. Fengge, and A. Jin-Woo, "Hybrid pole type bearingless switched reluctance motor with short flux path," in *Proceedings of the International Conference on Electrical Machines and Systems (ICEMS '11)*, pp. 1–6, Beijing, China, August 2011.

[10] Z. Xu, F. Zhang, and J.-W. Ahn, "Design and analysis of a novel 12–14 hybrid pole type bearingless switched reluctance motor," in *Proceedings of the 21st IEEE International Symposium on Industrial Electronics (ISIE '12)*, pp. 1922–1927, Hangzhou, China, May 2012.

[11] C. R. Morrison, "Bearingless switched reluctance motor," U.S. Patent 6727618 B1; April 2004.

[12] C. R. Morrison, M. W. Siebert, and E. J. Ho, "Electromagnetic forces in a hybrid magnetic-bearing switched-reluctance motor," *IEEE Transactions on Magnetics*, vol. 44, no. 12, pp. 4626–4638, 2008.

[13] C. Xin, D. Zhiquan, Z. Zheng, and Z. Lidan, "Principle and implementation of a bearingless switched reluctance generator with three adjacent excitation-windings connected in series," *Transactions of China Electrotechnical Society*, vol. 28, no. 2, pp. 108–116, 2013 (Chinese).

[14] M. Takemoto, K. Shimada, A. Chiba, and T. Fukao, "A design and characteristics of switched reluctance type bearingless motors," in *Proceedings of the 4th International Symposium on Magnetic Suspension Technology*, pp. 49–63, NASA/CP, Washington, DC, USA, May 1998.

[15] M. Takemoto, A. Chiba, H. Akagi, and T. Fukao, "Radial force and torque of a bearingless switched reluctance motor operating in a region of magnetic saturation," *IEEE Transactions on Industry Applications*, vol. 40, no. 1, pp. 103–112, 2004.

[16] M. Takemoto, H. Suzuki, A. Chiba, T. Fukao, and M. A. Rahman, "Improved analysis of a bearingless switched reluctance motor," *IEEE Transactions on Industrial Electronics*, vol. 37, pp. 26–34, 2001.

[17] X. Cao, Z. Deng, G. Yang, and X. Wang, "Independent control of average torque and radial force in bearingless switched reluctance motors with hybrid excitations," *IEEE Transactions on Power Electronics*, vol. 24, no. 5, pp. 1376–1385, 2009.

[18] T. W. Nehl, F. S. Fouad, and N. A. Demerdash, "Determination of saturated values of rotation machinery incremental and apparent inductances by an energy perturbation method," *IEEE Transactions on Power Apparatus and Systems*, vol. 101, no. 12, pp. 4441–4451, 1982.

[19] Y. Gang, *Basis research on a bearingless switched reluctance motor College of Automation Engineering [M.S. dissertation]*, Nanjing University of Aeronautics and Astronautics, Nanjing, China, 2008, (Chinese).